

DEGREE SCALE ANISOTROPY: SP94 RESULTS

J. O. Gundersen^{1,2}, M. Lim^{1,2}, J. Staren^{1,2}, C. A. Wuensche³, N. Figueiredo^{1,3,5}, T. C. Gaier^{1,2},
T. Koch⁴, P. R. Meinhold^{1,2}, M. D. Seiffert^{1,2}, G. Cook¹, A. Segale¹, P. M. Lubin^{1,2}

Received _____; accepted _____

Submitted to Astrophysical Journal Letters

arXiv:astro-ph/9412020v1 7 Dec 1994

¹Department of Physics, University of California, Santa Barbara, CA 93106

²NSF Center for Particle Astrophysics, University of California, Berkeley, CA 94720

³Instituto Nacional de Pesquisas Espaciais-INPE/MCT, Divisao de Astrofisica, Sao Jose dos Campos, SP, Brasil 12227-010

⁴Jet Propulsion Laboratory, California Institute of Technology, 4800 Oak Grove Drive, Pasadena, CA 91109

⁵Escola Federal de Engenharia de Itajuba, Departamento de Fisica e Quimica, Itajuba, MG, Brazil 37500-000

ABSTRACT

We present results from two observations of the cosmic microwave background (CMB) performed from the South Pole during the 1993-1994 austral summer. Each observation employed a 3° peak to peak sinusoidal, single difference chop and consisted of a $20^\circ \times 1^\circ$ strip on the sky near our SP91 observations. The first observation used a receiver which operates in 3 bands between 38 and 45 GHz (Q-band) with a FWHM beam which varies from 1° to $1^\circ 15'$. The second observation overlapped the first observation and used a receiver which operates in 4 bands between 26 and 36 GHz (Ka-band) with a FWHM beam which varies from $1^\circ 25'$ to $1^\circ 7'$. The Ka-band system has a similar beamsize and frequency coverage as the system used in our SP91 results. Significant correlated structure is observed in all bands for each observation. The spectrum of the structure is consistent with a CMB spectrum and is formally inconsistent with diffuse synchrotron and free-free emission at the 5σ level. The amplitude of the structure is inconsistent with 20 K interstellar dust; however, the data do not discriminate against flat or inverted spectrum point sources. The root mean square amplitude ($\pm 1\sigma$) of the combined (Ka+Q) data is $\Delta T_{rms} = 42.0_{-6.8}^{+15.8} \mu\text{K}$ for an average window function which has a peak value of 0.97 at $\ell = 68$ and drops to $e^{-0.5}$ of the peak value at $\ell = 36$ and $\ell = 106$. A band power estimate of the CMB power spectrum, C_ℓ , gives $\left\langle \frac{C_\ell \ell(\ell+1)}{2\pi} \right\rangle_B = 1.77_{-0.54}^{+1.58} \times 10^{-10}$. The band power estimates for the individual Ka and Q-band results are larger than but consistent with the band power estimate of the combined Ka-band SP91 results.

Subject headings: cosmic microwave background — cosmology: observations

1. Introduction

Anisotropy measurements of the cosmic microwave background (CMB) are a very effective tool for testing and constraining models of cosmic structure formation. With the discovery of large angular scale anisotropy by COBE (Smoot et al., 1992), there has been an increased interest in characterizing anisotropy on degree angular scales. Although all CMB measurements have to overcome a long list of systematic effects and foreground contaminants (Wilkinson, 1994), they have the potential to constrain many of the global parameters of the Universe and thus discriminate among the plethora of cosmic structure formation models. Over the past six years, we have travelled to the South Pole three times to perform these degree scale anisotropy measurements. The results from our 1988-89 measurements are detailed in Meinhold and Lubin, 1991 (SP89a) and Meinhold et al., 1993 (SP89b) while the results from the 1990-91 measurements are detailed in Gaier et al., 1992 (SP91a) and Schuster et al., 1993 (SP91b). The results from these measurements and the five balloon-borne Millimeter-wave Anisotropy eXperiment (MAX) are summarized in Lubin, 1994. In order to obtain additional data and frequency coverage, we returned to the Amundsen-Scott South Pole Station during the austral summer 1993-94.

2. Instrumentation

The SP94 observations used the Advanced Cosmic Microwave Explorer (ACME) as have all our previous degree scale anisotropy measurements. ACME is a one meter off axis Gregorian telescope which has been described in detail in SP89b. During the observations, the ellipsoidal secondary oscillated sinusoidally at 8 Hz with a peak to peak throw of 3° on the sky. The receiver signals were phase synchronously demodulated using a “square-wave” lockin amplifier and sampled every 0.5 seconds. The beam profile of the telescope can be approximated as a Gaussian beam with a $1 \sigma_b$ dispersion which varies in frequency as given below. Two different total power radiometers were used in these observations. The lower frequency (Ka-band) receiver is similar to that described in SP91a and incorporates a very low noise, high electron mobility transistor (HEMT) amplifier (Pospieszalski et al., 1990) cooled to 4 K in a ^4He dewar. This receiver operated at four center frequencies (27.25, 29.75, 32.25, and 34.75 GHz) with 2.5 GHz 3 dB bandwidths. The band subdivision is used to compensate for gain variations across the full band and to obtain spectral information which can be used to discriminate between the various astrophysical foregrounds. For the Ka-band system, the beam dispersion is given by $\sigma_b = 0.^\circ 70 \pm 0.^\circ 04 \times \left(\frac{27.7}{\nu_{GHz}} \right)$. The higher frequency receiver (Q-band) is described in Gundersen et al., 1994 and also uses a cryogenic HEMT amplifier based on a design developed at the National Radio Astronomy Observatory (NRAO). This amplifier was built at UCSB with assistance from NRAO and uses an AlInAs/GaInAs/InP HEMT (Pospieszalski et al., 1994) in the first of five amplification stages. The Q-band system was multiplexed into 3 equal bands centered at 39.15,

41.45, and 43.75 GHz with nominal 3 dB bandwidths of 2.3 GHz, and the beam dispersion is given by $\sigma_b = 0.^\circ47 \pm 0.^\circ04 \times \left(\frac{41.5}{\nu_{GHz}}\right)$. The HEMT amplifiers introduce intrinsic cross correlations between the bands which can be characterized by the correlation coefficient between any two frequencies. The measured correlations were typically 0.25 and 0.50 for the Ka and Q-band systems, respectively, including atmospheric correlations. The radiometers are calibrated to 10% absolute accuracy and 3% relative accuracy using a combination of cryogenic cold loads, the sky, ambient Eccosorb, and the Moon. The long term stability of the system was checked daily by inserting an ambient load “calibrator”. These calibrations varied by less than 3% over the time scale of an observation and contribute a negligible amount to the final error estimate.

3. Observations

Two observations were performed between January 9, 1994 and January 22, 1994 and collected 261 hours of data. The first observation used the Q-band receiver and the second observation used the Ka-band receiver. These observations consisted of smooth, constant declination, constant velocity scans of length 20° on the sky about a center $\alpha_{cen} = 45^\circ$, $\delta_{cen} = -62^\circ$. The closest approach to the Sun was 60° on the sky and the closest approach to the plane of the galaxy corresponds to $b^{II} = -40^\circ$, $l^{II} = 272^\circ$. This is a low foreground emission region which overlaps some of the region observed in SP91. Our measurement of the Eta Carina region showed that our absolute elevation was one degree lower than we expected. The offset has been attributed to sag in the inner frame of the telescope mount and makes a direct comparison between these measurements and the SP91 measurements problematic. The instantaneous right ascension of the beam for any of the 3 observations can be given by $\alpha(t) = \alpha_{cen} + 20(S(t) \bmod 2 - 1/2) / \cos \delta_{cen} + \alpha_o \sin(2\pi\nu_{ch}t) / \cos \delta_{cen}$ where $S(t) = int(\nu_{sc}t + 1)$ enumerates the scan number, $\alpha_o = 1.5^\circ$ is the sinusoidal chop amplitude, $\nu_{ch} = 8$ Hz is the chop frequency, and $\nu_{sc} = 10$ mHz is the scan frequency. The instantaneous beam position on the sky is then given by $\varphi(t) = \alpha(t) \cos \delta_{cen}$. Observations of the Moon established the absolute pointing at low elevations and this was confirmed with observations of Eta Carina at high elevations. The error in absolute pointing is $\pm 0.25^\circ$ in right ascension and $\pm 0.12^\circ$ in declination while the error in relative pointing is $\pm 0.05^\circ$ in right ascension and $\pm 0.05^\circ$ in declination. If a temperature at position \hat{n}_i^k is compared to a temperature at position \hat{n}_j^l at the same declination, then the dimensionless window function can be written as

$$W_\ell(\Phi_{ij}^{kl}) = B_\ell(\sigma_b^k)B_\ell(\sigma_b^l) \sum_{r=0}^{\ell} \frac{(2\ell - 2r)!(2r)!}{[2^\ell r! (\ell - r)!]^2} 4H_0^2[(\ell - 2r)\alpha_o] j_0^2[(\ell - 2r)\Delta\varphi/2] \cos[(\ell - 2r)\Phi_{ij}^{kl}] \quad (1)$$

where $\Phi_{ij}^{kl} = \cos^{-1}(\hat{n}_i^k \cdot \hat{n}_j^l)$ is the angular difference (or lag) between the temperature measured at bin i with channel k and the temperature measured at bin j with channel l . The beam profile function is given by $B_\ell(\sigma_b) = \exp[-\ell(\ell + 1)\sigma_b^2/2]$, H_0 is the Struve function of 0 index, j_0 is

the 0^{th} order spherical Bessel function and $\Delta\varphi = (20/43)(\pi/180)$ is the bin size in radians on the sky. The indices are given by $i, j = 1$ to $N = 43$ bins and $k, l = 1$ to $F = 3$ for the Q-band data and $k, l = 1$ to $F = 4$ for the Ka-band data. This window function is shown in Figure 2 for the different combinations of beamsizes and is a specific example taken from a more general expression in White and Srednicki (1994).

4. Data Reduction and Analysis

Data were rejected for a number of reasons including poor pointing/chopper performance (1.2%), performance of other observations (0.2%), calibration sequences (0.7%), telescope/receiver maintenance (9.1%), temperature variations of the cold plate and backend electronics (0.9%), and bad weather (12.9%). From a total of 261 hours of data, 196 hours were used in the data analysis. The poor weather data were determined in a way similar to SP91b in which the data from a single scan were combined into position bins from which an average and one sigma error bar were calculated. The χ^2 of the individual scans was then calculated, and if the probability of exceeding χ^2 for 43 degrees of freedom was less than 0.01 for any channel, then the data from *all* channels for that scan were removed. As a cross check, other weather filters similar to SP91a were also implemented with no significant changes in the final data set. As with SP89 and SP91, an offset and gradient were removed in time over the time scale of a single scan (100 secs) for each of the channels in an observation. The offsets were between 1 and 2 mK depending on the channel. The offset and gradient subtraction are taken into account in the analysis by creating a matrix R such that $\tilde{T}_a^k = R_{aj}^{kl} T_j^l$ where T_j^l are the $F \times N$ temperature means and \tilde{T}_a^k are the $F \times (N - 2)$ projected temperatures with $a = 1, N - 2$. The formation of R is discussed in Bunn et al. 1994 and we have made R orthogonal such that $R^T R = I$. The coadded means and 1 sigma error bars are shown in Figure 1 and show statistically significant, correlated signals for each observation. All quoted temperatures have been converted from antenna temperature to thermodynamic temperature and have been corrected for atmospheric absorption. In order to determine the origin of the observed structure, the data were binned in azimuthal and heliocentric coordinate systems. Various subset analyses were performed including dividing the data set into four roughly equal quarters in time and dividing the data into four roughly equal quarters depending on the azimuthal position of the telescope beam. None of these analyses suggest that the observed structure is anything but celestial in origin.

5. Astrophysical Foregrounds

There are several astrophysical foregrounds which could contaminate these observations. These include diffuse synchrotron and free-free emission from within our own galaxy and

extragalactic emission from discrete radio sources. Neither the Sunyaev-Zeldovich effect nor diffuse 20 K dust emission is expected to contribute more than a few μK signal. If we assume that the 408 MHz map (Haslam et al.) is a tracer of diffuse, high galactic latitude synchrotron emission, then we calculate the rms differential synchrotron emission to be 1.0 K at 408 MHz for these observations. Given the spectral index for diffuse synchrotron is $\beta = -2.8$ with an antenna temperature given by $T_A \propto \nu^\beta$, we estimate that the diffuse synchrotron contribution to the observed rms to be $< 7 \mu\text{K}$ in the lowest frequency channel and $< 3 \mu\text{K}$ in the highest frequency channel. The small amount of differential emission that exists in this region of the sky at 408 MHz can be correlated with discrete radio sources which have been observed in other source surveys at 408 MHz and are identified in the PKSCAT90 database (Wright and Otrupcek, 1990). Unlike diffuse synchrotron emission, discrete radio sources and free-free emission cannot be dismissed on amplitude arguments alone. For diffuse free-free emission, there are no all-sky surveys which would allow a direct estimate of the free-free contribution to the observed structure. Instead, we have to rely on estimates based on a $10^\circ \times 12^\circ$ $\text{H}\alpha$ map (Reynolds, 1992) made at a similar angular scale to predict an average background free-free brightness temperature that can be expressed as $T_{ff} = 1 \times 10^{-2} \nu_{\text{GHz}}^{-2.1} \text{csc} |b^{\text{II}}|$. Reynolds' data suggests that the variations in the $\text{H}\alpha$ intensity may be a factor of 2 above the average, such that $\Delta T_{ff} = 2T_{ff}$. From this we calculate the differential brightness temperature due to free-free emission (upon the closest approach to the galactic plane) to range from $\Delta T_{ff} = 30 \mu\text{K}$ at the lowest frequency to $\Delta T_{ff} = 12 \mu\text{K}$ at the highest frequency. There have been many discrete source surveys at lower frequencies which are compiled in the PKSCAT90 database. The Parkes-MIT-NRAO (PMN) survey at 4.85 GHz (Wright et al., 1994) serves as the most sensitive survey with a flux limit of 30 mJy in our observation region and includes all the sources identified in PKSCAT90 for our region. The sensitivity of the telescope is $90 \mu\text{K}/\text{Jy}$ (assuming 100% aperture efficiency), so a 30 mJy flat spectrum source (with a flux density $S(\text{Jy}) \propto \nu^{\beta+2} \propto T_A \nu^2$, $\beta = -2$) would produce a $3 \mu\text{K}$ signal, which is well below the noise of the observations. Since the effective solid angle, Ω_e , of the telescope varies like $\Omega_e \propto \nu^{-2}$, a flat spectrum point source with a solid angle $\Omega_p \ll \Omega_e$ and $T_{flat} \propto \nu^{-2}$ would give $T_A = \Omega_p \frac{T_{flat}}{\Omega_e} \propto \nu^0$, while a thermal point source produces an antenna temperature $T_A \propto \nu^2$. If we make the worst case assumption that all the point sources have flat spectra to 45 GHz, then we estimate that they would produce a $\Delta T_{rms} = 30 - 45 \mu\text{K}$. Since the worst case estimates of contamination from free-free emission and flat spectrum point sources are comparable to the rms level of the observed structure, we cannot dismiss or verify these types of foreground contamination without measuring β . This is addressed in the following likelihood analysis.

6. Likelihood Analysis

We use the Bayesian method with a uniform prior (Bond et al. 1991) in the determination of the root mean square (rms) amplitude of the data and to make an estimate of the broad-band

power in the CMB power spectrum (Bond, 1994a, and Steinhardt, 1994). The experimental two point correlation function is given by

$$C(\hat{n}_i^k \cdot \hat{n}_j^l) = \left\langle \frac{\Delta T(\hat{n}_i^k) \Delta T(\hat{n}_j^l)}{T_0^2} \right\rangle = \frac{1}{4\pi} \sum_{\ell=2}^{\infty} (2\ell + 1) C_\ell W_\ell(\Phi_{ij}^{kl}) \quad (2)$$

where $\langle a_{\ell m} a_{\ell' m'} \rangle = \delta_{\ell\ell'} \delta_{mm'} C_\ell$ for a spherical harmonic expansion of the radiation temperature given by $\frac{\Delta T(\hat{n})}{T_0} = \sum_{\ell m} a_{\ell m} Y_{\ell m}(\hat{n})$, W_ℓ is the window function (Eq. 1) and $T_0 = 2.726 \pm 0.01$ K (Mather et al. 1994). The rms amplitude is calculated from

$$\left(\frac{\Delta T}{T_0} \right)_{rms}^2 = \frac{1}{4\pi} \sum_{\ell=2}^{\infty} (2\ell + 1) C_\ell \bar{W}_\ell, \quad \bar{W}_\ell = \frac{1}{N_{pix}} \sum_{ikl} W_\ell(\Phi_{ii}^{kl}) \quad (3)$$

where $N_{pix} = F^2 \times N$ and \bar{W}_ℓ is the average window function at zero lag. Following Bond, 1994a, the broad band power estimate is given by

$$\langle \bar{C}_\ell \rangle_B = \left\langle \frac{C_\ell \ell(\ell + 1)}{2\pi} \right\rangle_B = \frac{(\Delta T/T_0)_{rms}^2}{\sum_{\ell=2}^{\infty} (\ell + \frac{1}{2}) \bar{W}_\ell / (\ell(\ell + 1))}. \quad (4)$$

We consider a scale invariant, $n = 1$, “flat” radiation power spectrum given by $C_\ell \propto (f^k f^l)^\beta / (\ell(\ell + 1))$ where the constant of proportionality and β are determined in the likelihood analysis and f^k is the center frequency of channel k normalized to the lowest center frequency of the observation(s). The full covariance matrix is given by $M_{ij}^{kl} = C(\hat{n}_i^k \cdot \hat{n}_j^l) + D_{ij}^{kl} \sigma_i^k \sigma_j^l / T_0^2$ where $D_{ij}^{kl} \sigma_i^k \sigma_j^l$ is the data covariance matrix which is diagonal in each of the $F^2 N \times N$ submatrices. This covariance matrix accounts for all spatial and channel-channel correlations as well as the error for each bin at each frequency. The offset and gradient subtraction are taken into account by creating a projected covariance matrix given by $\tilde{M} = R M R^T$, where R is defined in Section 4. The likelihood of the data set is proportional to $|\tilde{M}|^{-1/2} \exp(-\chi^2/2)$, where $\chi^2 = \tilde{T}^T \tilde{M}^{-1} \tilde{T}$ for $F \times (N - 2)$ degrees of freedom. Table 1 lists the resulting rms and band power estimates for the individual observations as well as the combined observations. Figure 2 shows the band power estimates with $\beta = 0$ in relation to the COBE band power estimate.

7. Discussion

The Q-band broad band power is consistent with standard CDM normalized to COBE and has a spectral index, β , which is consistent with the CMB spectrum. The Ka-band observation is also consistent with standard CDM normalized to COBE; however, the spectral index does not rule out discrete radio sources and thus does not afford such a straightforward interpretation. When the Ka and Q-band data are combined, the broad band power is consistent with the standard CDM model normalized to COBE and the spectral index is consistent with the CMB

spectrum. For the standard CDM power spectrum, the amplitude of the combined Ka+Q observations corresponds to a $Q_{rms-PS} = 16.2_{-2.6}^{+5.4} \mu\text{K}$. The combined Ka+Q data show a marked improvement on the 1σ confidence interval for the best fit β . For the most probable ΔT_{rms} , spectra with $\beta < -2$ (such as diffuse synchrotron and free-free emission) are formally excluded at the 5σ level. The SP94 results are most easily compared to the SP91 results and the results of Wollack et al. 1993 (SK93). A reanalysis (Bond, 1994b) of the combined SP91a and SP91b observations gives $\langle \overline{C}_\ell \rangle_B = 1.06_{-0.27}^{+0.83} \times 10^{-10}$ which compares to the Ka-band SP94 results of $\langle \overline{C}_\ell \rangle_B = 1.17_{-0.42}^{+1.33} \times 10^{-10}$. The Bond, SP91 analysis assumes that $\beta = 0$ and that there is no channel to channel correlations. The SK93 result gives $\langle \overline{C}_\ell \rangle_B = 1.31_{-0.7}^{+1.2} \times 10^{-10}$, for $\beta = -0.3_{-1.2}^{+0.7}$. The SK93 result is consistent with both the SP94 and the combined SP91 results, although one should note the differences between the experiments which are addressed in SK93.

We would like to thank M. Pospieszalski, M. Balister, and W. Lakatosh of NRAO-CDL for useful information regarding amplifiers and for supplying the 26-36 GHz HEMT amplifier. In addition we would like to thank L. Nguyen of Hughes Research Labs for providing the InP HEMTs which we've incorporated into our 38-45 GHz amplifiers. This project would have been impossible without the support of B. Sadoulet and the Center for Particle Astrophysics. D. Fischer and the whole Antarctic Support Associates staff provided the valuable support and expertise at the Amundsen-Scott South Pole station. We are grateful to N. Sugiyama for providing us with the CDM radiation power spectrum and to R. Bond, M. Srednicki, P. Steinhardt, M. White, and L. Page for useful discussions regarding data analysis and window functions. We would like to acknowledge the previous contributions of J. Schuster. N. Figueiredo is partially supported by Conselho Nacional de Desenvolvimento Cientifico e Tecnologico, Brazil. This work was supported by NSF grant OPP 92-21468 and AST 91-20005.

The means, covariances and window functions will be made available from rot.ucsb.edu using anonymous FTP in the directory [sp94dat] and from the Web site <http://www.deepspace.ucsb.edu>.

Table 1. Derived Parameters From Likelihood Analysis ($\pm 1\sigma$)

| Band | ΔT_{rms} (μK) | β | ΔT_{rms} (μK) | $\left\langle \frac{C_\ell \ell(\ell+1)}{2\pi} \right\rangle_B$ $\times 10^{-10}$ |
|---------|---------------------------------------|---------------------|---------------------------------------|--|
| (1) | (2) | (3) | (4) | (5) |
| Q-band | $42.8^{+16.9}_{-7.3}$ | $1.7^{+1.5}_{-1.6}$ | $49.3^{+19.3}_{-8.3}$ | $2.14^{+2.00}_{-0.66}$ |
| Ka-band | $30.8^{+14.7}_{-6.1}$ | $0.2^{+0.9}_{-1.4}$ | $32.0^{+14.7}_{-6.5}$ | $1.17^{+1.33}_{-0.42}$ |
| Ka+Q | $31.9^{+11.6}_{-6.1}$ | $0.9^{+0.3}_{-0.6}$ | $42.0^{+15.8}_{-6.8}$ | $1.77^{+1.58}_{-0.53}$ |

Note. — (cols. [2-3]) The rms amplitude and spectral index β determined from the likelihood analysis using a scale invariant, $n=1$, “flat” radiation power spectrum given by $C_\ell \propto (f^k f^l)^\beta / (\ell(\ell + 1))$, where f^k is the center frequency of channel k normalized to the lowest frequency of the observation; (col. [4]) the rms amplitude for $\beta = 0$; (col. [5]) CMB broad-band power spectrum estimate for $\beta = 0$.

REFERENCES

- Bond, J. R., et al. 1991, Phys. Rev. Lett., 66, 2179
- Bond, J. R. 1994a, CITA-94-5, preprint
- . 1994b, (private communication)
- Bunn, E, et al. 1994, ApJ, 429, L1
- Gaier, T., et al. 1992, ApJ, 398, L1
- Gorski, K. M., et al. 1994, ApJ, 430, L89
- Gundersen, J. O., et al. 1994, Proc. of the Case Western CMB Workshop
- Haslam, C. G. T., et al. 1982, A&AS, 47, 1
- Lubin, P. M., 1994, Proc. of IAU 168
- Mather, J., et al. 1994, ApJ, 420, 439
- Meinhold, P., & Lubin, P. 1991, ApJ, 370, L11
- Meinhold, P., et al. 1993, ApJ, 406, 12
- Pospieszalski, M. W., Gallego, J. D., & Lakatos, W. J. 1990, IEEE MTT-S Digest 1253
- Pospieszalski, M. W., et al. 1994, Proc. of the International Microwave Symposium, 1345
- Schuster, J., et al. 1993, ApJ, 412, L47
- Smoot, G. F., et al. 1992, ApJ, 396, L1
- Steinhardt, P. J. 1994, Proc. of the 1994 Snowmass Workshop on Particle Astrophysics and Cosmology, eds. E. Kolb and R. Peccei
- Sugiyama, N. 1994, private communication
- White, M. & Srednicki, M. 1994, ApJ, in press (astro-ph/9402037)
- Wilkinson, D. 1994, Proc. of the 1994 Lake Louise Winter Institute
- Wollack, E. J., et al. 1993, ApJ, 419, L49
- Wright, A. E., & Otrupcek, R. E., eds. 1990, ATNF, “PKSCAT90-The Southern Radio Database” (Sydney: ATNF)

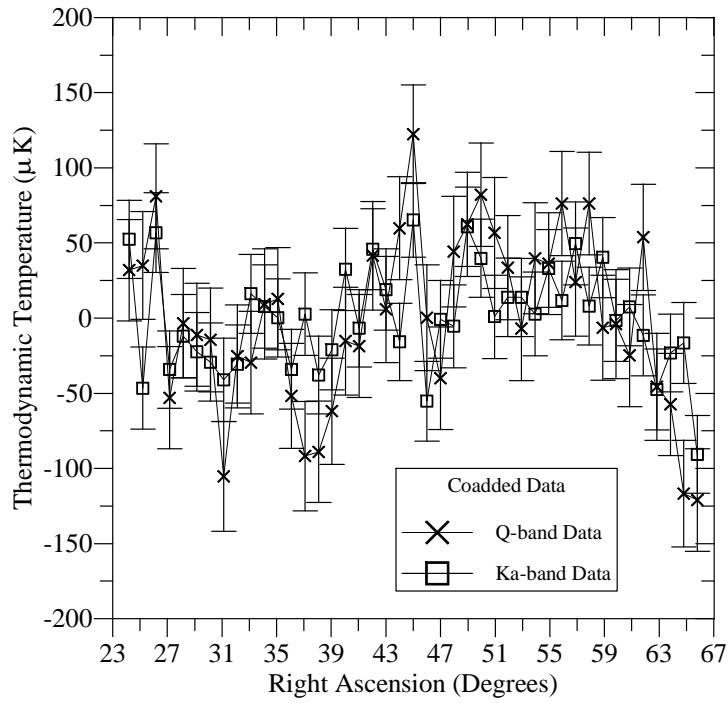


Fig. 1.— Coadded single difference data in μK thermodynamic temperature, referenced to the top of the atmosphere with $\pm 1\sigma$ error bars. The error bars account for the correlated noise between the channels. The data in this figure shows that there is significant correlated structure. This data set was not explicitly used in the analysis since the spatial correlations between the bins have to be taken into account using the full theoretical covariance matrix.

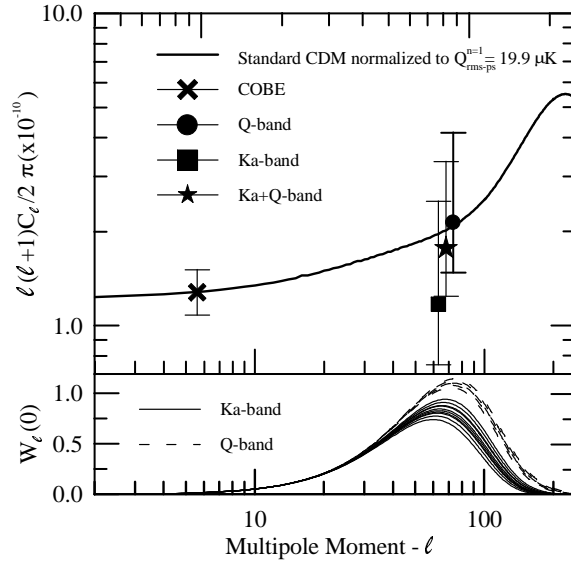


Fig. 2.— The top figure shows the band power estimates as given in Table 1 compared to the standard CDM radiation power spectrum (Sugiyama, 1994) normalized to the COBE $Q_{rms-ps}^{n=1} = 19.9 \pm 1.6 \mu K$ (Gorski et al., 1994). The lower figure shows the window function at zero lag for the Q and Ka-band receivers. The different traces represent the window functions for the various combinations of beamsizes for each receiver. The combined Ka+Q-band window function is not shown for clarity sake.